

pubs.acs.org/acsapm Article

# Influence of Solvent Affinity on Transport through Cross-Linked Copolymer Membranes for Organic Solvent Nanofiltration

Michael P. Dugas, Shukun Zhong, Bumjun Park, Jizhou Jiang, Jonathan A. Ouimet, Jialing Xu, Jennifer L. Schaefer, and William A. Phillip\*



Cite This: ACS Appl. Polym. Mater. 2023, 5, 6781-6794



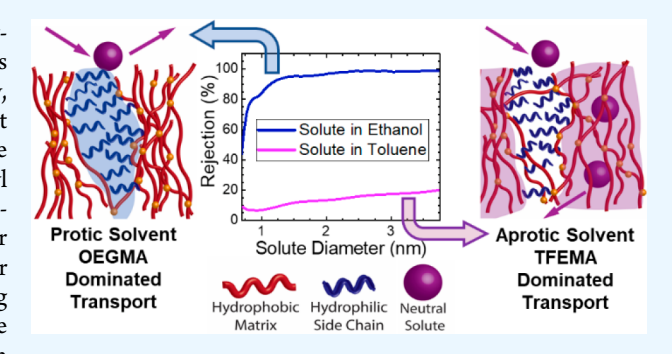
**ACCESS** I

III Metrics & More

Article Recommendations

sı Supporting Information

ABSTRACT: Membranes based on microphase-separated copolymers offer an opportunity to address the need for resilient materials that can be used in organic solvent-based filtration. Specifically, copolymer repeat unit chemistries can be chosen to impart solvent compatibility, to tailor membrane nanostructure, and to enable postsynthetic modification. In this study, a poly(trifluoroethyl methacrylate-co-oligo(ethylene glycol) methyl ether methacrylate-co-glycidyl methacrylate) [P(TFEMA-OEGMA-GMA)] copolymer was synthesized and fabricated into flat sheet and hollow fiber membranes using a non-solvent-induced phase separation casting technique. The GMA repeat units possess epoxide groups that were used to cross-link the copolymer through a ring-opening reaction



with diamines ranging from diaminoethane to diaminooctane. Transport experiments in water, methanol, ethanol, tetrahydrofuran, dimethylformamide, and toluene demonstrated that films reacted with longer diamines, such as diaminohexane, result in stable membranes. Conversely, the films reacted with shorter diamines degraded upon exposure to organic solvents. Because of their stability in organic solvents, transport through the diaminohexane-functionalized membranes was characterized in more detail using hydraulic permeability and neutral solute rejection experiments. The results of these experiments along with volumetric swelling and small-angle X-ray scattering (SAXS) analysis revealed that the solvent affinity for the constituent copolymer domains is critical in determining the permeation pathway. For P(TFEMA-OEGMA-GMA) membranes in protic solvents, such as ethanol, transport through the hydrophilic side chains of OEGMA was favored, while for membranes in aprotic solvents, such as toluene, transport through the hydrophobic matrix dominated. In neutral solute rejection experiments, 2000 g mol<sup>-1</sup> polypropylene glycol molecules (solvated size ~2 nm) permeated through the hydrophobic domain unhindered but were fully rejected when permeation occurred through the hydrophilic region. These differences highlight the need to understand the interactions between the copolymer domains and solvent when solvent-resilient membranes are developed for organic solvent filtration.

KEYWORDS: copolymer membrane, organic solvent nanofiltration, neutral solute rejection, solubility parameter, Flory-Huggins

#### 1. INTRODUCTION

Organic solvent nanofiltration (OSN) can help meet the need for energy-efficient separation in organic solvent environments. Currently, 10% of society's daily energy use is consumed by separation processes. Moreover, these processes account for 40–70% of the capital and operating costs for a chemical plant. Membranes have become an integral part of water purification and desalination due to their energy efficiency and simple operation. A key aspect of this integration is the stability of polymeric membranes in aqueous solutions. However, organic solvents will often dissolve conventional membranes, disrupting their nanostructure and rendering them incapable of any separation. Therefore, resilient membranes are needed to withstand harsh chemical conditions and ultimately to expand their use in industrial processes.

The recognized need for solvent-stable OSN membranes has driven research into cross-linkable homopolymers, such as

diamine-cross-linked polyimides. <sup>5–8</sup> This approach enhances solvent stability, demonstrating that cross-linking is a viable route toward solvent-stable membranes. However, cross-linking often reduces membrane throughput and the use of homopolymer materials presents an additional limitation, as the surface chemistry and nanostructure of these polymer membranes cannot be easily tailored for specific separation processes.

Membranes that are constructed of microphase-separated copolymers have shown promise in a variety of applications

Received: March 6, 2023 Accepted: July 24, 2023 Published: August 9, 2023





Figure 1. Reaction schematic of the copolymerization of P(TFEMA-OEGMA-GMA). The weight percentage of each monomer and the percentage of initiator are also indicated.

due to their well-defined nanostructures and tunable functionality. The copolymer material is designed using varied repeat units with oligomeric side chains that are chemically incompatible with the polymer backbone.9 The balance between the enthalpic desire of the constituent repeat units to phase separate and their entropic desire to avoid chain stretching results in these copolymer membranes assembling into a continuous network of nanopores between 2 and 5  $\,\mathrm{nm.}^{10-14}$  Moreover, through synthetic control of the macromolecular chemistry, the pore wall chemistry of copolymer membranes can be altered to increase the strength of the membrane through cross-linking as well as to tailor the membrane for specific separations.  $^{10-12,15,16}$  Relevant examples are detailed in reports regarding the fabrication of membranes from a statistical poly(trifluoroethyl methacrylateco-oligo(ethylene glycol) methyl ether methacrylate-co-glycidyl methacrylate) (P(TFEMA-OEGMA-GMA)) copolymer. 11,1 After casting the P(TFEMA-OEGMA-GMA) copolymer into membranes using both a blade-casting and dip-coating technique, the oxirane groups of the glycidyl methacrylate moieties that line the pore walls are allowed to react with hexamethylenediamine to incorporate positively charged ammonium moieties and cross-link the membrane. Notably, as evidenced by transport experiments as well as nanostructure characterizations, the well-defined nanostructure of the copolymer materials was retained throughout the functionalization process and even after permeating ethanol, which dissolved the copolymer before cross-linking. 11 However, the effect of the cross-linker identity on the nanostructure of the membrane was not explored. In addition, other organic solvents were not investigated for this copolymer material.

In this study, P(TFEMA-OEGMA-GMA) copolymer membranes were investigated to understand the changes in nanostructure due to the solvent environment. The effect of the cross-linker identity on the nanostructure was investigated by using varying lengths of diamines. The effective cross-linking was determined through gel fraction and water solvent permeability cycling experiments. The transport of solvent through the membrane was elucidated through permeability and volumetric swelling experiments. The results of these experiments were correlated to chemical properties, such as molar volume and Flory—Huggins interaction parameters, to help understand the behavior of copolymer membranes in varied solvent environments. The correlations between the nanostructure and transport behavior of the membranes was

further analyzed using small-angle X-ray scattering (SAXS), neutral solute rejections, and permeability studies. Finally, the membranes were subjected to dye rejection experiments to compare the results of neutral solute rejection experiments with those observed for solutes that are commonly used in OSN membrane evaluations. These experiments demonstrate that by evaluating the physical and chemical properties of repeat units in a copolymer, the solvent environment, and the postfabrication functionalization process, resilient copolymer-based OSN membranes can be fabricated. Importantly, the characterization across scales reveals information that can be used to further advance the design of polymers for membrane-based OSN applications.

#### 2. MATERIALS AND METHODS

2.1. Materials. All materials were purchased from Sigma-Aldrich unless noted otherwise. Trifluoroethyl methacrylate (TFEMA), oligo(ethylene glycol) methyl ether methacrylate ( $M_n$  500 g mol<sup>-1</sup>) (OEGMA), and glycidyl methacrylate (GMA) were used as monomers. 2,2'-Azobis(2-methylpropionitrile) (AIBN) was the free radical initiator. Toluene and chloroform were the solvents for polymerization and purification, respectively, while hexane was the nonsolvent. Trifluoroethanol was the solvent for membrane casting, and isopropyl alcohol (IPA) (VWR) was used as the nonsolvent. Poly(vinylidene difluoride) (PVDF) hollow fiber (HF) membranes with nominal pore diameters of 40 nm (donated by Dow Chemical, currently Dupont) were used as supports for HF membranes, while poly(trifluoroethylene) (PTFE) flat sheet (FS) membranes with reported pore diameters of 0.2  $\mu$ m were purchased from Sterlitech. Dopamine and tris(hydroxymethyl)aminomethane (Tris) buffer were used to polymerize an interfacial layer of polydopamine on the PTFE membranes. DI water was purified in a Milli-Q 18.2 M $\Omega$  filtration system. Ethylenediamine (diaminoethane), 1,3-diaminopropane (diaminopropane), 1,4-diaminobutane (diaminobutane), hexamethylenediamine (diaminohexane), and 1,8-diaminooctane (diaminooctane) were the diamine cross-linkers. Silicon wafers (University Wafers), sodium dodecyl sulfate (SDS), (3-aminopropyl)triethoxysilane (APTES), hydrochloric acid, and methanol (MeOH) were used to produce samples for swelling experiments. Kapton tape (VWR) and 1.0 mm special glass capillary tubes (Charles Supper) were utilized in the small-angle X-ray scattering (SAXS) analysis. Ethanol (EtOH), tetrahydrofuran (THF), dimethylformamide (DMF), and toluene were used as solvents for transport experiments. Poly(propylene glycol) (PPG) of different molecular weights (M<sub>n</sub> 425, 725, 1000, 2000, 2700, and 4000 g mol<sup>-1</sup>) as well as Martius Yellow, Rose Bengal, and Crystal Violet were used in solute rejection experiments.

**2.2. Copolymer Synthesis.** The P(TFEMA-OEGMA-GMA) copolymer was synthesized using a free-radical copolymerization. 10,11

The monomers TFEMA, OEGMA, and GMA were passed through basic alumina columns to remove any inhibitors and then added to a flask at a monomer composition of 40% TFEMA, 40% OEGMA, and 20% GMA by weight. The reaction flask also contained toluene and 0.5% AIBN (by moles of monomers). The solution was heated to 60 °C and then allowed to react for 20 h under a nitrogen environment. Figure 1 shows a schematic of the copolymerization reaction. The resulting copolymer was then precipitated in hexane, dried under vacuum, and purified twice using chloroform as a solvent and hexane as a nonsolvent. A Bruker Ascend 400 proton nuclear magnetic resonance spectrometer (H NMR) and a Waters gel permeation chromatograph (GPC) with Polymer Standard Services columns (guard, 105, 103, and 102 Å SDV) and refractive index detector calibrated with poly(methyl methacrylate) standards were used to determine the composition and molecular weight of the copolymer, respectively.

**2.3.1.** *Dip-Coated Hollow Fiber.* HF membranes were fabricated using a previously reported dip-coating technique. <sup>11</sup> A 2% (by weight) solution of polymer dissolved in trifluoroethanol was dispensed into a Teflon dye. The HF support was pulled through the dye at a translational speed of 0.5 cm s<sup>-1</sup>. The solvent was allowed to evaporate for 5 min 10 s starting from the instant the HF began to move through the dye. The HF was then inverted and submerged in an IPA nonsolvent bath at 0.5 cm s<sup>-1</sup> to ensure a consistent solvent evaporation time across the length of the membrane. After casting, the membrane was allowed to stay submerged in the nonsolvent bath for 1 h before proceeding to functionalization and testing.

2.3.2. Blade-Casted Flat Sheets. Flat sheet membranes were bladecast using a methodology adapted from previous works. <sup>11,15,19</sup> Polydopamine was polymerized on the surface of the PTFE substrate prior to casting to create a stable interfacial layer. A basic buffer solution was prepared by dissolving 50 mM Tris hydrochloride in DI water. Then, the pH of the solution was measured using a Fischer Accumet AP115 pH meter with a 13-620-AP50A probe and adjusted to pH 8.5 using 1 M NaOH and 1 M HCl solutions. The dopamine solution was prepared by dissolving 2 mg mL<sup>-1</sup> dopamine chloride into the buffer solution. <sup>20,21</sup> Approximately 20 mL of the dopamine solution was placed into a Petri dish followed by laying a 8 cm × 8 cm sample of PTFE substrate on top of the solution. The substrate was left on top of the solution for 18 h, after which it was removed and rinsed thoroughly with DI water. The substrate was then allowed to dry between two glass slides to keep the film flat.

A 20% (by weight) casting solution was prepared by dissolving the copolymer into trifluoroethanol. The solution was passed through a 1  $\mu$ m glass syringe filter and then allowed to degas overnight. A transfer pipet was used to dispense 1–2 mL of the casting solution onto the dopamine-prepared PTFE substrate. A doctor blade set at a gate height of 63  $\mu$ m above the substrate was used to draw the solution into a thin film. The solvent was allowed to evaporate for 5 min before the membrane was plunged into the IPA nonsolvent bath, where the membrane was submerged for approximately 1 h. The membrane was transferred to DI water for long-term storage.

**2.4. Epoxide—Amine Functionalization.** Reactive solutions of diamines, ranging from diaminoethane to diaminooctane, were prepared by dissolving each diamine into DI water to create a 1 M solution. The casted membranes were submerged into the diamine solutions and allowed to react for at least 3 h at room temperature. Figure S2 shows a schematic of a diamine reacting with an epoxide ring lining the pore wall of a membrane. The molar ratio of diamines to epoxide rings from the GMA was in significant excess (>>10:1) to ensure the complete reaction of epoxide rings with amines. After the reaction, the membranes were rinsed with and stored in DI water.

**2.5. Membrane Characterization.** *2.5. 1. Functionalization and Cross-Linking.* Samples were placed under vacuum for a minimum of 2 h prior to analysis. X-ray photoelectron spectroscopy (XPS) analysis was performed utilizing a Phi VersaProbe II instrument with MultiPak software. The samples were analyzed for C, N, O, and F. The spectra were shifted on the basis of the location of the 286 eV C—C peak. The N spectrum was analyzed in an attempt to determine the extent of

cross-linking by quantifying the relative intensities of the peaks associated with primary and secondary amines. <sup>22</sup> Fourier transform infrared (FTIR) analysis was performed with a Bruker Tensor 27 ATR-FTIR. The samples were scanned 64 times from 400 to 4500 cm $^{-1}$  at a resolution of 4 cm $^{-1}$ . The spectra were normalized with a C=O peak at approximately 1725 cm $^{-1}$ . The peaks of interest located at 908 and 1580 cm $^{-1}$  are associated with the stretch of the epoxide ring and the bend of the amine group, respectively.  $^{10,11}$ 

2.5.2. Nanostructural Analysis. Scanning electron microscopy (SEM) analysis was conducted by using a Magellan 400 FEI microscope. Samples were placed under a vacuum overnight before being fixed on studs using carbon tape. Cross-section samples were submerged and broken in liquid nitrogen before being placed on the studs, with the membrane surface perpendicular to the stud surface. All of the samples were sputter-coated with iridium and electrically grounded to the stud with colloidal silver. Micrographs were taken at several points for each sample using an electron gun setting of 5 kV and 6.3 pA with the instrument in immersion mode.

SAXS measurements were obtained at Argonne APS synchrotron beamline 12-ID-B, operated by the Chemical and Materials Science group at Argonne National Laboratory, at room temperature with an X-ray beam wavelength of 0.9322 Å (energy of 13.3 keV). The copolymer material was blade cast onto a Kapton FS film using the casting parameters described above. The films were then reacted with diaminopropane, diaminohexane, and diaminooctane as detailed in the reactive film section. The reacted films were cut into 1 mm wide, 2 cm tall strips and placed in special glass capillary tubes. The tubes were filled with 20  $\mu$ L of the desired solvent to submerge the sample and capped with epoxy resin.

2.5.3. Swelling and Gel Fraction Characterization. Two different techniques were utilized to quantify the swelling behavior of the copolymer films. Bulk swelling experiments were conducted by blade casting a 20% (by weight) polymer solution onto glass plates. The glass plates were first treated with 1 M KOH to prevent adhesion of the membrane. After casting, the solvent was allowed to evaporate completely (~15 min), and then the copolymer film was plunged into a water bath. The films were reacted with diaminohexane overnight and soaked in water for 24 h to remove any excess reactant. The films were cut into circular samples using a 5/8 in. arc punch, placed in weighed scintillation vials, and weighed to determine the mass of the water-swollen film. 5 mL of an organic solvent (i.e., MeOH, EtOH, IPA, THF, DMF, toluene, or hexane) was placed inside the vial. The vials were sealed with a screw cap, and the films were allowed to equilibrate for 5 days. For toluene, which is immiscible with water, the copolymer films were submerged in IPA for 24 h to exchange with water before initiating a swelling experiment. The solvent volume was selected to assume 99.9% purity. For toluene swelling, the films were submerged in IPA first for 24 h to wick away the water. The films were patted lightly dry and then submerged in 5 mL of toluene for 5 days. Afterward, the dimensions of the membrane were measured by using a Dino-Lite digital microscope.

Ellipsometry was also employed to quantify swelling. Silicon wafers were surface-reacted with APTES to incorporate amine groups onto the surface using an adapted procedure from the literature.<sup>23</sup> The wafers were submerged in 2% (w/v) aqueous SDS solution for 24 h and then rinsed with water, dried with Kim wipes, and exposed to ozone from a Jetlight Model 18 ozone generator for 10 min. The wafers were then submerged in a 1:1 volume ratio of hydrochloric acid and MeOH for 30 min at room temperature. The wafers were washed and immersed in EtOH for 5 min. The silicon was soaked in 5% (v/v) APTES in EtOH for 20 min, rinsed with EtOH, and then submerged in MeOH for 48 h to remove any excess APTES. Once the wafers were reacted with APTES, a 500  $\mu L$  aliquot of 2 wt % copolymer casting solution was spin coated onto the silicon at a speed of 3000 rpm for 30 s using a Cee Apogee spin coater. The film and silicon were placed on a stir plate at 60 °C overnight to react the exposed amine groups from the APTES with the epoxide rings on the bottom of the spin-coated film. The films were then reacted with a diamine solution for 3 h, rinsed with water, and dried under vacuum before being subjected to experiments. Using a J.A. Woollam Alpha

SE ellipsometer, we measured the films in a dry state first to determine the base thickness of the film. Three different positions were measured to determine the average thickness of the sample. The samples were then subjected to the various organic solvents and allowed to swell for 1 h. The excess solvent was removed from the surface of the sample, and the thickness was measured again. Solvent was applied to the film between measurements to avoid solvent evaporation as much as possible.

Gel fraction measurements were conducted to determine the cross-linking of the copolymer membranes. Films fabricated from 20 wt % polymer solutions were cast and reacted with diaminohexane or diaminopropane using the procedure described in the volumetric swelling study. The membranes were then dried in a vacuum oven at room temperature for at least 12 h, and the mass of the dried film was taken. The copolymer material was then placed in a vial containing excess DMF and continually stirred for 24 h. The DMF was decanted from the copolymer, and the films were rinsed 3 times with DI water. The material was dried under vacuum for at least 12 h, and the mass of the residual film was taken. The gel content was calculated using the equation

$$g = \frac{m_{\rm r}}{m_{\rm i}} \times 100\% \tag{1}$$

where g is the gel content in percent,  $m_r$  is the dry mass after exposure to DMF, and  $m_i$  is the initial dry mass.

**2.6.** Membrane Transport Behavior. 2.6.1. Permeability and Cycling Experiments. HF membranes were cut to a length of 10 cm and secured into a home-built module. Circular samples of the FS membranes were cut using a 2 in. arc punch and placed inside a Sterlitech HP 4750 stainless steel stirred cell with Teflon O-rings and gaskets. These modules were used for the duration of the experiments described below.

Permeability experiments were conducted with the HF membranes for EtOH and FS membranes for MeOH, IPA, THF, DMF, hexane, and toluene. Water permeabilities were measured for all membranes prior to any organic solvent permeation. Once the membranes were secured in the modules, the feed solvent was added to the stirred cell for FS setup or the reservoir tank for the HF system.<sup>11</sup> Pressure was then applied across the membranes to initiate the experiment. The applied pressure difference was kept at approximately 10 psi for HF membranes and 55 psi for FS membranes. The membranes were allowed to permeate the solvent for over 2 h to ensure the system reached steady state. The permeate was then collected for approximately 10 min using scintillation vials covered with Parafilm to prevent evaporation. The mass of the permeate was recorded over time, and the mass flow rate  $(\dot{m}_p)$  along with the applied pressure difference ( $\Delta P$ ), the membrane area ( $A_{\rm m}$ ), and the density of the solvent  $(\rho)$  were utilized to calculate the liquid permeability  $(L_p)$  as shown in eq 2:

$$L_{\rm p} = \frac{\dot{m}_{\rm p}}{\rho A_{\rm m} \Delta P} \tag{2}$$

Solvent cycling experiments were conducted by using a modified version of the technique described above. Water was permeated through the membranes for 2 h to determine the initial permeability. The feed was then immediately changed to the organic solvent, and the permeate was collected and weighed over the course of 2 h to monitor the change in permeability. The feed was replaced with water again, and the hydraulic permeability was monitored for 2 h. This process was repeated for four additional cycles to determine the durability of the membrane. Afterward, the membranes were thoroughly permeated with water and stored in DI water to remove any excess solvent that may have remained within the membrane structure.

2.6.2. Neutral Solute Rejections. Neutral solute rejection experiments were performed to establish the molecular weight cutoff curves for the copolymer membranes in each solvent. Five different molecular weights of PPG ranging from 400 to 4000 g mol<sup>-1</sup> were dissolved equally into the target solvent. The feed solutions were

formulated to contain 0.2 g  $\rm L^{-1}$  of each PPG sample (i.e.,  $M_{\rm n}=425$ , 725, 1000, 2000, and 4000 g  $\rm mol^{-1}$ ) such that the total polymer concentration was 1 g  $\rm L^{-1}$ . Approximately 5 mL of pure solvent was permeated through the membranes to prevent contamination between experiments. After the pure solvent permeation, 120 mL of the PPG-containing solution was placed in the feed reservoirs. The feed solution was stirred at 200 rpm to prevent concentration polarization. Approximately 1 mL of the initial permeate was discarded to prevent any contamination of the pure solvent and the neutral solute permeate. The permeate was collected using scintillation vials topped with Parafilm to reduce evaporation. At the conclusion of the experiment, the retentate solution in the feed reservoir was collected for analysis.

Samples of the feed, permeate, and retentate solutions were prepared for analysis by GPC. 1 mL of each solution was pipetted into scintillation vials, which were placed under vacuum for 48 h to allow all the solvent to evaporate. Afterward, 1 mL of HPLC grade THF was placed in the scintillation vial to redissolve the samples. The samples were spiked with 20  $\mu$ L of a 10 g L $^{-1}$  poly(ethylene glycol) (PEG,  $M_{\rm n}=35000~{\rm g~mol}^{-1}$ ) in toluene solution. Subsequently, the results of the GPC analysis were normalized using the intensity measured for the  $M_{\rm n}=35000~{\rm g~mol}^{-1}$  PEG internal standard. Percent rejection (R) was calculated using the intensity, which is proportional to concentration,  $^{24,25}$  of the permeate  $(I_{\rm p})$  and feed  $(I_{\rm F})$  as shown in eq 3:

$$R = \left(1 - \frac{I_{\rm p}}{I_{\rm F}}\right) \times 100\% \tag{3}$$

2.6.3. Dynamic Light Scattering (DLS). DLS analysis was performed to determine the relationship between the MW and the solute diameter of the PPG as a function of solvent. PPG of a specific MW was dissolved in the desired solvent. The sample was filtered using a 0.4  $\mu$ m PTFE syringe filter and placed in a quartz cuvette. The samples were analyzed by using a Malvern Nano-ZS with a backscatter detector. The Zetasizer software calculated the volume average size of the polymer in solution, and the solute diameter was plotted as a function of MW and solvent. The best line of fit was calculated using a power law to determine the correlation between the MW and solute diameter. The solute diameter was utilized to determine the pore diameter in the neutral solute rejection experiments using a hindered transport equation from the literature.  $^{26}$ 

2.6.4. Dye Rejections. Dye molecules are often used to assess solute rejection and pore size of OSN membranes. Here, the dye rejections of Martius Yellow, Crystal Violet, and Rose Bengal were studied to compare the rejections of the dyes and similarly sized neutral solutes. Single-solute feed solutions were generated by dissolving each dye at a concentration of  $25~\mu g~L^{-1}$  in the organic solvent of interest. These dye solutions were utilized as feed solutions in rejection experiments, which used techniques similar to those for neutral solute experiments.

The concentrations of the dye in the feed and permeate solutions were then analyzed using a Cary 60 spectrophotometer. The instrument was corrected for background by using the pure solvent in a quartz cuvette. The absorbance spectra were collected on the survey setting from 800 to 200 nm. The rejection was then calculated eq 3 using the intensity of the peaks at 426 nm for Martius Yellow, 590 nm for Crystal Violet, and 562 nm for Rose Bengal.

#### 3. RESULTS AND DISCUSSION

**3.1.** Copolymer Design, Synthesis, and Characterization. The P(TFEMA-OEGMA-GMA) copolymer is designed to produce membranes with a TFEMA matrix, a water-permeable OEGMA domain, and reactive epoxide rings from GMA lining the pore walls. <sup>10,11,15,27</sup> GPC and <sup>1</sup>H NMR analyses were used to determine the molecular weight and composition of the material, respectively. Figure S1 shows the <sup>1</sup>H NMR and GPC analyses for one of the three copolymer batches used in the study. <sup>1</sup>H NMR analysis of all three

batches indicated that the average compositions of the copolymers, based on weight percentages, were  $52.1 \pm 5.5\%$  TFEMA,  $24.9 \pm 4.6\%$  OEGMA, and  $23.0 \pm 0.9\%$  GMA. GPC analysis also indicated that the molecular weight of the copolymers was  $102 \pm 2.8$  kg mol<sup>-1</sup>. These results are similar to previous work conducted with this copolymer. <sup>11,17</sup> The small sample-to-sample variation suggests that the polymerization produced the target copolymer reliably.

3.2. Reproducible Fabrication of Copolymer Membranes. The casting process facilitates the formation of nanostructured membranes. The P(TFEMA-OEGMA-GMA) copolymer is dissolved in trifluoroethanol to create a homogeneous solution that is then cast as a thin film on a substrate. The trifluoroethanol is allowed to evaporate, which results in the polymer concentration at the solution-air interface increasing. As the concentration increases, the enthalpic repulsion between the copolymer backbone and the OEGMA side chains drives the microphase separation that templates the nanostructure of the membrane. Plunging the membrane into a nonsolvent bath solidifies the polymer, fixes the nanostructure of the active layer in place, and allows for the remaining solvent to be removed. This casting process has been used to create nanofiltration membranes in both the HF and FS configurations. 10,11,17

HF membranes were cast using a dip-coating method that deposits a thin film of the casting solution on commercial HF supports. Specifically, using a home-built Teflon die, the HF support is pulled through a 2% (by weight) copolymer solution. After solvent evaporation and plunging the membrane in the nonsolvent bath, this process creates  $\sim 250$  nm thick copolymer film, as seen in Figure 2A. <sup>11,28</sup> The membranes produced in this manner had an average hydraulic permeability for water of 6.7  $\pm$  1.1 L m<sup>-2</sup> h<sup>-1</sup> bar<sup>-1</sup> (n=3 membranes).

FS membranes were fabricated using a blade casting technique. PTFE substrates were chosen due to their chemical compatibility with the organic solvents used in the subsequent experiments. The PTFE substrate, shown in Figure 3A,D, had larger pores (~200 nm) than PVDF FS substrates (~50 nm) that were used in prior reports. 11,17 The large pore diameters as well as the chemical affinity between PTFE and trifluoroethanol resulted in the casting solution wicking into the pores of the as-received substrates. This wicking created a nonuniform active layer with defects that rendered the membrane ineffective. To address this issue, an interfacial polydopamine layer was formed on top of the PTFE support. After an 18 h reaction time, the membrane turned a tan color (Figure 3B), and an additional layer of material was observed on the surface of the PTFE substrate through SEM analysis (Figure 3E). Figure 4 shows the FTIR spectra for the asreceived and dopamine-treated PTFE substrate. The appearance of a broad peak at 1580 cm<sup>-1</sup>, which is consistent with the amine groups in polydopamine, suggests that dopamine was polymerized on the PTFE surface.

After the PTFE substrate was modified with polydopamine, FS membranes could be cast reliably from 20% (by weight) copolymer solutions. The resulting membrane and surface structure are shown in Figures 3C and 3F, respectively. The surface of the membrane, as seen in Figure 3F, is featureless, which is consistent with a defect-free selective layer that is formed during the casting process. SEM micrographs of the membrane cross section revealed that the increased polymer concentration resulted in thicker copolymer films (Figure 2B)

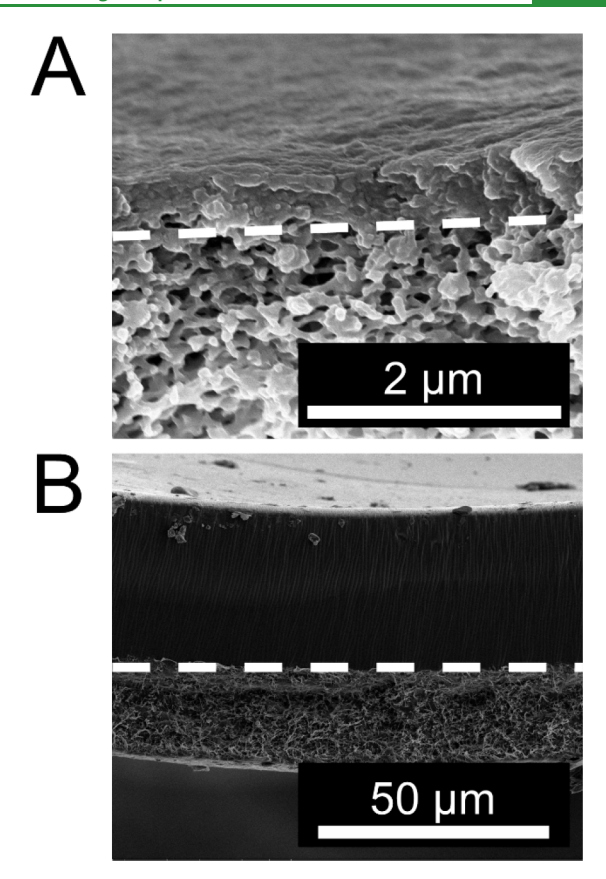


Figure 2. (A) Cross-section SEM micrograph of a P(TFEMA-OEGMA-GMA) HF membrane. The porous structure of the PVDF HF substrate is shown below the dashed line. (B) Cross-section SEM micrograph of an FS membrane. The copolymer layer of the membrane is cast directly on the surface of the polydopamine-treated PTFE support. The microstructure of the PTFE support is displayed below the dashed line while the copolymer layer is situated above the dashed line.

that exhibited a reduced hydraulic permeability of  $2.9 \pm 1.3$  L m<sup>-2</sup> h<sup>-1</sup> bar<sup>-1</sup> (n = 3). However, the membranes were stable when they were used in permeability and solute rejection experiments.

**3.3. Diamine Functionality Affects Membrane Performance.** A base-catalyzed epoxide ring-opening reaction was used to functionalize the copolymer membranes with a series of diamines. <sup>10,19,22</sup> Prior work demonstrated that, in addition to introducing positively charged functional groups along the pore walls, this reaction cross-links the copolymer material resulting in membranes that withstand operation in ethanol. <sup>11</sup> This work explores this phenomenon further by investigating the influence of the diamine length on the stability and transport characteristics of copolymer membranes in a variety of organic solvents.

FTIR and XPS analyses were used to monitor the fabrication process as well as the membrane functionalization reaction. Figure 4 shows the FTIR spectra for a flat sheet membrane through each step of the fabrication process. The bottom spectrum is from the PTFE support as received from the manufacturer. When polydopamine is polymerized on the surface, a broad peak can be seen at  $\sim 1580~\rm cm^{-1}$ . This peak corresponds to the N–H bend from the amine functional groups. The FTIR profile changes when the copolymer material is cast on top of the polydopamine layer, as seen in

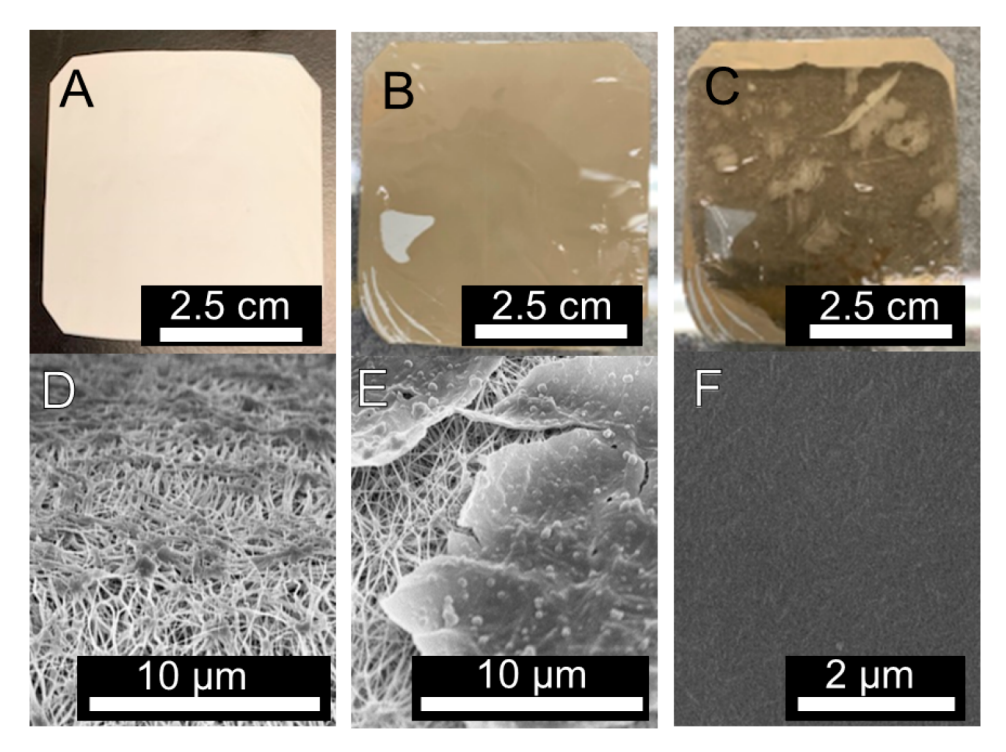
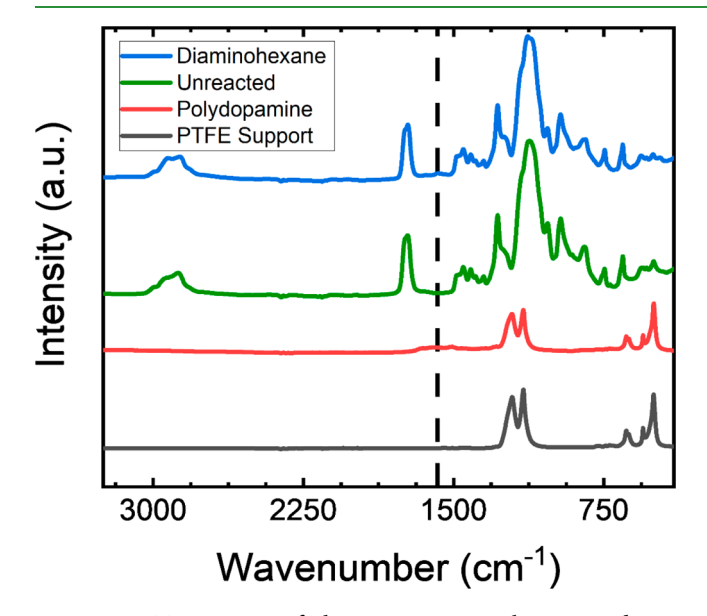


Figure 3. FS membranes in different stages during the casting process. Panels A–C display the macroscopic features of the membrane, and panels D–F report the membrane nanostructure, as observed using SEM analysis. (A) PTFE substrate as received from the manufacturer. (D) SEM micrograph showing the pore structure of the PTFE films that had a manufacturer reported nominal pore diameter of 200 nm. (B) Substrate after undergoing a surface polymerization of polydopamine. (E) SEM micrograph showing the polydopamine polymerized on the surface of the support. (C) Membrane after the copolymer layer was deposited on top of the polydopamine-treated PTFE substrate. (F) Surface SEM micrograph of the copolymer membrane.



**Figure 4.** FTIR spectra of the composite copolymer membrane during the fabrication process. The bottom spectrum (black) is that of the PTFE substrate. The spectrum in red corresponds to the PTFE substrate after an 18 h interfacial polymerization with polydopamine. The green spectrum is from the copolymer layer casted on top of the polydopamine. Lastly, the blue spectrum shows a diaminohexane-reacted copolymer membrane. The amine peaks from the polydopamine layer and the diaminohexane-functionalized membrane at 1580 cm<sup>-1</sup> are labeled with the dashed line.

the green spectrum in Figure 4. The shoulder peak at 908 cm<sup>-1</sup>, which is associated with the epoxide ring stretching, is

observed only in the spectrum for the unreacted parent film The upper spectrum belongs to the copolymer layer that is functionalized with diaminohexane. A small N–H bending peak at 1580 cm<sup>-1</sup> appears in this spectrum, which suggests that the epoxide rings reacted with the diamines. Similar results were observed for FTIR spectra from polymeric films reacted with diamines of varying lengths (Figure S3).

XPS analysis was also executed to characterize the reaction between the epoxide rings and diamines. Figure S4 shows the N spectra for the parent and diamine-reacted membranes as well as the analysis of the peaks. The two peaks observed in the spectra for the diamine-reacted samples correspond to primary (399 eV) and secondary (401 eV) amines. The presence of the peak associated with secondary amines, which result from the ring-opening reaction, indicate that the diamines reacted with the epoxide rings inside the membrane structure.<sup>22,29</sup> Ideally, the XPS spectra could be used to quantify the extent of crosslinking within the membrane. However, the current analysis showed an abundance of primary amines due to unreacted diamines that were not sufficiently rinsed from the samples prior to analysis. Nevertheless, both FTIR and XPS analyses help demonstrate that the membranes were functionalized with diamines.

The durability of the copolymer membranes in organic solvent environments was interrogated by measuring the hydraulic permeability of samples that were cycled repeatedly between DI water and organic solvent feed solutions. Figure 5 shows the results of EtOH—water cycling experiments that were conducted with HF membranes functionalized with diaminopropane or diaminohexane. The solid points in the figure represent the hydraulic permeability measured for DI

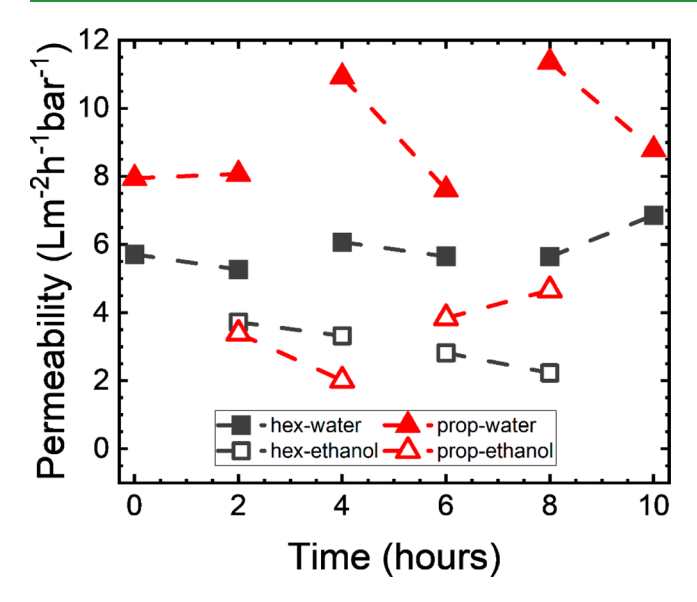


**Figure 5.** Ethanol/water cycling experiments conducted using HF copolymer membranes functionalized with diaminopropane (propane) and diaminohexane (hex). The applied pressure was approximately 12.5 psi. Each permeation cycle lasted 4 h (2 h with water, 2 h with EtOH). Permeate was collected for approximately 10 min at each point in the plot and weighed to determine permeability. The solid points are the water permeabilities while the outlined points are the EtOH permeabilities. The dashed lines are to help guide the eye from one point to the next chronologically.

water, while the outlined points represent the hydraulic permeability measured for EtOH. The lines connecting the points are provided to help guide the eye. For membranes reacted with diaminohexane, the EtOH permeabilities remained approximately half the value measured for water with each cycle. For example, the water and EtOH permeabilities for the diaminohexane reacted membranes were  $5.8 \pm 0.7$  and  $3.5 \pm 0.2$  L m<sup>-2</sup> h<sup>-1</sup> bar<sup>-1</sup>, respectively. The stability of the permeability measurements demonstrates that the membranes do not degrade in EtOH. The membranes reacted with diaminopropane, on the other hand, exhibited a large increase in the permeability of water (11.1  $\pm$  0.3 L m<sup>-2</sup> h<sup>-1</sup> bar<sup>-1</sup>) when they were first transitioned from EtOH to water. The hydraulic permeability decreased back to the original value (8.0  $\pm$  0.1 L m<sup>-2</sup> h<sup>-1</sup> bar<sup>-1</sup>) as the water continued to permeate for 2 h.

Similar to the ethanol results, the diaminohexane-reacted films were stable in THF, DMF, and toluene, while the diaminopropane sample degraded as the cycling experiments progressed. Figure S6 shows the results from these cycling experiments conducted with the FS membranes. Each membrane was subjected to a sequence of THF, DMF, and toluene cycling experiments, and the results were plotted as a function of time (Figure S6). For all the solvents, the diaminohexane-functionalized films exhibit rapid responses to the exchange of the solvent and stable permeabilities following the exchange. Table 1 summarizes the hydraulic permeabilities observed for the diaminohexane-functionalized membrane throughout the cycling experiments. The hydraulic permeability of water does not change significantly as the solvents are exchanged, which is consistent with the copolymer layer remaining intact during these experiments.

The performance of the diaminopropane-reacted membrane, on the other hand, degraded continually throughout the

Table 1. Average Permeabilities for Water and Solvents for Diaminohexane-Reacted Films throughout the Cycling Experiments<sup>a</sup>

solvent	water permeability $(L m^{-2} h^{-1} bar^{-1})$	solvent permeability $(L m^{-2} h^{-1} bar^{-1})$
THF	$2.2 \pm 0.2$	$1.2 \pm 0.3$
DMF	$2.3 \pm 0.2$	$0.95 \pm 0.3$
toluene	$2.4 \pm 1.0$	$1.0 \pm 0.5$

"The errors correspond to the standard deviation from all of the points in the solvent cycling experiment.

cycling experiments. The hydraulic permeability for water at the beginning of the experiment was  $1.45 \pm 0.6 \text{ L m}^{-2} \text{ h}^{-1}$ bar<sup>-1</sup>. The hydraulic permeability for THF throughout the experiment was stable at  $1.6 \pm 0.6 \text{ L m}^{-2} \text{ h}^{-1} \text{ bar}^{-1}$ . After THF was exchanged for water, the membrane initially had a high hydraulic permeability (23.1  $\pm$  3 L m<sup>-2</sup> h<sup>-1</sup> bar<sup>-1</sup>) that stabilized to a value of 12.4 ± 2 L m<sup>-2</sup> h<sup>-1</sup> bar<sup>-1</sup>, suggesting a change to the membrane structure after exposure to THF. After the THF experiment, the diaminopropane-reacted film exhibited a dramatic reduction in permeability independent of solvent identity. Moreover, the permeability value remained constant at a value of  $0.3 \pm 0.2 \text{ L m}^{-2} \text{ h}^{-1} \text{ bar}^{-1}$  as the solvents were exchanged. The low hydraulic permeability suggests that the copolymer material remained attached to the substrate, as opposed to previous studies where unreacted P(TFEMA-OEGMA-GMA) membranes dissolved into EtOH causing a dramatic increase in the permeability.<sup>27</sup> The shifts in the permeabilities for membranes reacted with diaminopropane compared to films reacted with longer diamines provide evidence that the length of the diamine affects the stability of the copolymer membrane in different solvent environments. This stability is likely related to the extent of cross-linking within the copolymer membranes.

Gel content experiments were conducted to further understand the influence of diamine chain length on membrane cross-linking. As seen in the cycling experiments, membranes reacted with diaminopropane were less stable compared to films reacted with diaminohexane. This result led to the hypothesis that the longer chain length diamines had a higher cross-link density. To test this hypothesis, gel fraction measurements were taken for films cross-linked with either diaminopropane or diaminohexane. For diaminopropanereacted films, the gel content was  $58.4 \pm 0.5\%$ . The diaminohexane-reacted material, on the other hand, had a gel content of 96.9  $\pm$  0.5%. These results further suggest that diaminohexane cross-linked the film more effectively than diaminopropane. The difference in cross-linking is consistent with the difference in transport behavior observed in the cycling experiments. The combined results indicate that for these copolymer membranes, longer cross-linkers stabilize the copolymer membrane more than shorter chained cross-linkers. Based on the results of the gel content and cycling experiments, diaminohexane-functionalized membranes were used throughout the rest of the study.

**3.4. Functionality and Solvent Environment Affect Membrane Transport.** The hydraulic permeabilities of the diaminohexane-functionalized membranes for a series of solvents are compared in Figure 6. Ethanol permeation experiments were conducted primarily using HF membranes while the other organic solvents (i.e., MeOH, IPA, THF, DMF, toluene, and hexane) were studied in the FS membrane

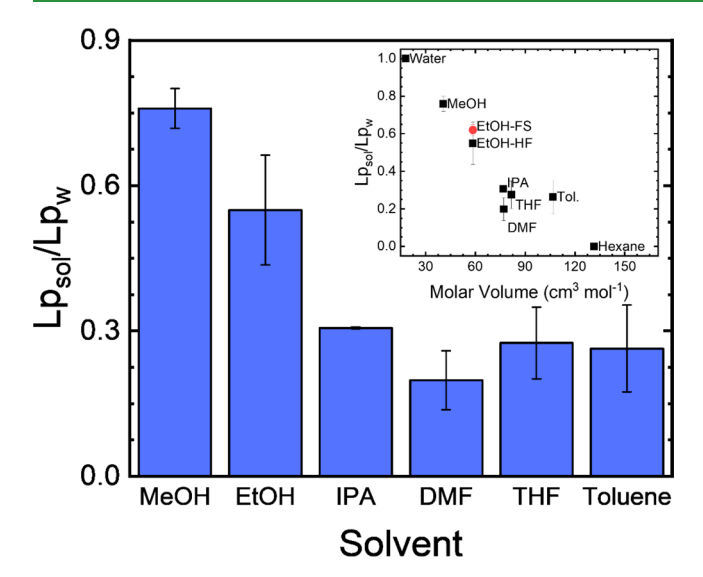


**Figure 6.** Permeability measurements of diaminohexane membranes in different solvents. The *y*-axis plots the permeability factor, which is the permeability normalized by the initial water permeability. Each permeability factor is the average of n=3 measurements. The permeability of ethanol was measured for both HF (black square) and FS (red circle) membranes, while the permeability of the other organic solvents was measured only with FS membranes Inset: permeability factor was plotted as a function of solvent molar volume.

configuration. To compensate for the difference in membrane thickness between the HF and FS configurations, Figure 6 reports the hydraulic permeability of the solvent normalized by the hydraulic permeability of water for the same sample. In this study, this ratio is termed the permeability factor. FS EtOH permeation experiments were conducted and compared to the HF EtOH permeation results. A permeability factor of  $0.55 \pm 0.1$  was calculated for EtOH-HF while the EtOH-FS permeation experiments yielded a permeability factor of  $0.62 \pm 0.03$ . These values are within experimental error, indicating that this normalization approach accounts for the differences in absolute permeability that result from differences in membrane thickness.

Hexane is not reported in Figure 6 because its permeability was below the limit of detection for the current apparatus.

As observed in the inset of Figure 6, the permeability factors tend to decrease as the molar volume of the solvent increases. <sup>30,31</sup> By itself, this information is not sufficient to identify the dominant transport mechanism through the membrane. For example, the molar volume and viscosity for similarly structured molecules (e.g., alkanes) are correlated. However, as demonstrated in Figure S8C, the solvent viscosity and permeability factor are not obviously correlated as suggested by a pore flow mechanism. <sup>32–34</sup> Alternatively, in a solution-diffusion mechanism, <sup>18,35–38</sup> the permeability coefficient is proportional to the diffusion coefficient of the solvent within the membrane. <sup>37,38</sup> In this case, for a membrane with a fixed free volume, the diffusion coefficient decreases as the molecular volume increases, which would lead to a decrease in permeability. <sup>39</sup>

Flory-Huggins  $\chi$  parameters, which quantify the interactions between solvents and the copolymer repeat units, were used to assess how solvent-membrane interactions influence solvent permeation. 41-44 Typically, membranes used in the OSN applications are made from homopolymers. In these instances, more favorable interactions between polymer and solvent, indicated by a smaller  $\chi$  parameter, correlate with higher hydraulic permeabilities while solvents with higher  $\chi$ parameter values exhibit a lower permeability due to unfavorable polymer–solvent interactions. 45–47 In this study, there are distinct nanostructured domains within the membrane whose constituent components can interact with the permeating solvents differently. As such, the permeability factors for each solvent were plotted versus the calculated Flory-Huggins  $\chi$  parameters (Table S3) for the TFEMA and OEGMA repeat units in Figure 7. For TFEMA (Figure 7A), the permeability factor increases as the  $\chi$  parameter increases. For OEGMA (Figure 7B), two distinct trends appear based on the protic or aprotic nature of the solvent. For aprotic solvents, represented by the red circles in Figure 7, the permeability factors decrease as the  $\chi$  parameter values increase. On the other hand, protic solvents, indicated by the blue circles, exhibit relatively favorable interactions with the OEGMA domains as indicated by  $\chi$  parameter values less than 0.6.

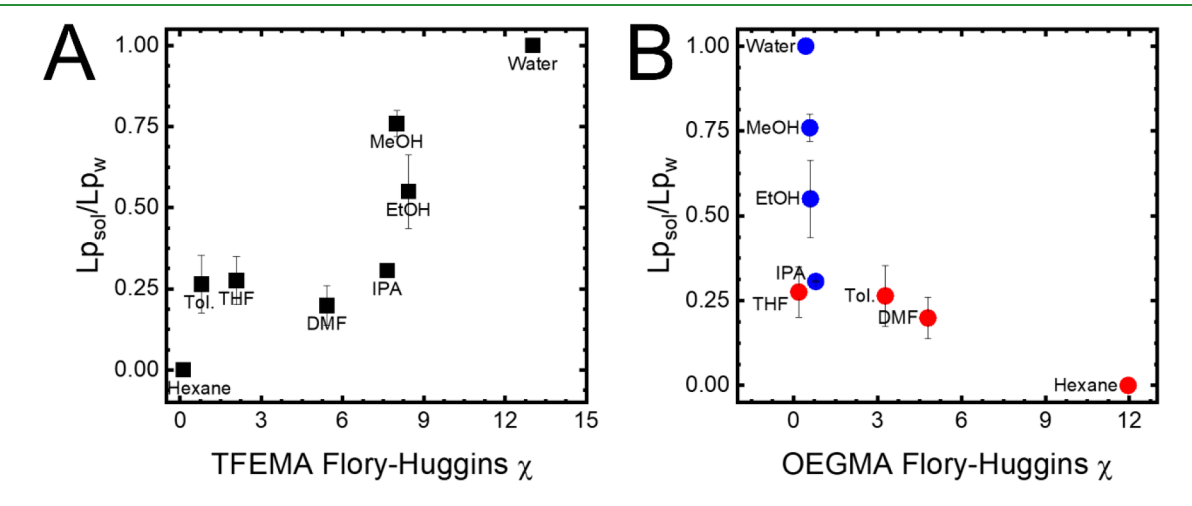


**Figure 7.** Permeability factor plotted as a function of the Flory–Huggins  $\chi$  parameters. (A) Flory–Huggins  $\chi$  parameters for TFEMA and organic solvents. (B) Flory–Huggins  $\chi$  parameters for OEGMA and the organic solvents. The blue points are for protic solvents that can hydrogen bond with OEGMA. These  $\chi$  parameters for protic solvents are taken from the literature <sup>40</sup> and those for aprotic solvents were calculated as detailed in the Supporting Information. The errors are standard deviations from n=3 measurements.

These solvents, water and alcohols, are capable of forming hydrogen bonds, which allows the solvent to structure along the oligomeric OEGMA side chains. <sup>41,48–50</sup> This solvent structuring can act as a lubricating layer, allowing the bulk of the solvent to pass relatively unhindered. <sup>51,52</sup>

Two trends emerge from the analysis of the permeability factors as a function of the Flory—Huggins  $\chi$  parameters. First, the lowest observed permeability factors corresponded with aprotic solvents that interact favorably with TFEMA and unfavorably with OEGMA. Second, higher permeability factors were observed for protic solvents that display an ability to hydrogen bond with OEGMA and unfavorable interactions with TFEMA. These results support a hypothesis that transport through the OEGMA domain dominates the behavior of the membrane for protic solvents.

Ellipsometry and volumetric swelling experiments were conducted to quantify the swelling behavior of the copolymer membranes as a function of the solvent environment. Figure S9 shows the results of the ellipsometry analysis, which allowed for the swelling behavior to be observed on a length scale similar to that of the copolymer layer in the permeability experiments. The thickness of the solvent-swollen samples were normalized to the dry film thickness. Most of the solvents had a minimal effect on the film thickness, swelling in a range of 1.0–1.7 times the dry film thickness. DMF swelled every membrane the most. The results for the un-cross-linked parent film were sporadic and not reproducible, suggesting the samples were dissolving into solution during the experiments.

Volumetric swelling experiments on bulk samples were conducted to further understand the swelling behavior on a larger scale (Figure S10). For these experiments, thick copolymer discs functionalized with diaminohexane were solvated, and the area of the solvent-swelled sample was compared to the area of the water-swelled material. Similar to the results from the ellipsometry analysis, the difference in the swelling between samples is not significant, with the films swelling by a factor of 1–1.5. These factors are lower compared to several polymeric films exposed to organic solvents in the literature, which can swell by a factor of 4 or more. <sup>47,53,54</sup> The volume swelling analysis indicates that the cross-linking from the diamines limits the amount of solvent that can be incorporated within the copolymer membrane.

3.5. Elucidating Solvent Effects on Copolymer Membrane Nanostructure. Neutral solute rejection experiments were used to investigate the nanostructure of the membrane as a function of the solvent identity. Dye rejection experiments were initially conducted in an attempt to assess the membrane nanostructure (Figure S12). 18,53,55 However, upon visual inspection following the experiments (Figure S13), it was clear that the dye molecules were poor model solutes for assessing membrane nanostructure because they adsorb to the membranes, leading to high rejection values independent of their molecular size. In contrast, neutral solutes of known diameter are filtered from solution based on their size relative to the diameter of the region responsible for transport. Subsequently, theories for hindered transport can be used to determine the feature size of the permeable domains. PPG, with molecular weights ranging from 425 to 4000 g mol<sup>-1</sup>, was selected as the neutral solute in this study due to its solubility in the solvents examined, its ability to assume a uniform shape in solution, and its minimal interactions with the membrane surface. 56-58 The MW of PPG was correlated to its hydrodynamic diameter in each solvent through DLS. DLS

measures the diffusion coefficient of the solute, which is then utilized to determine the solute size through the Stokes—Einstein equation. The results of this analysis, which are reported in Figure 8A, show that the solute diameter ranged

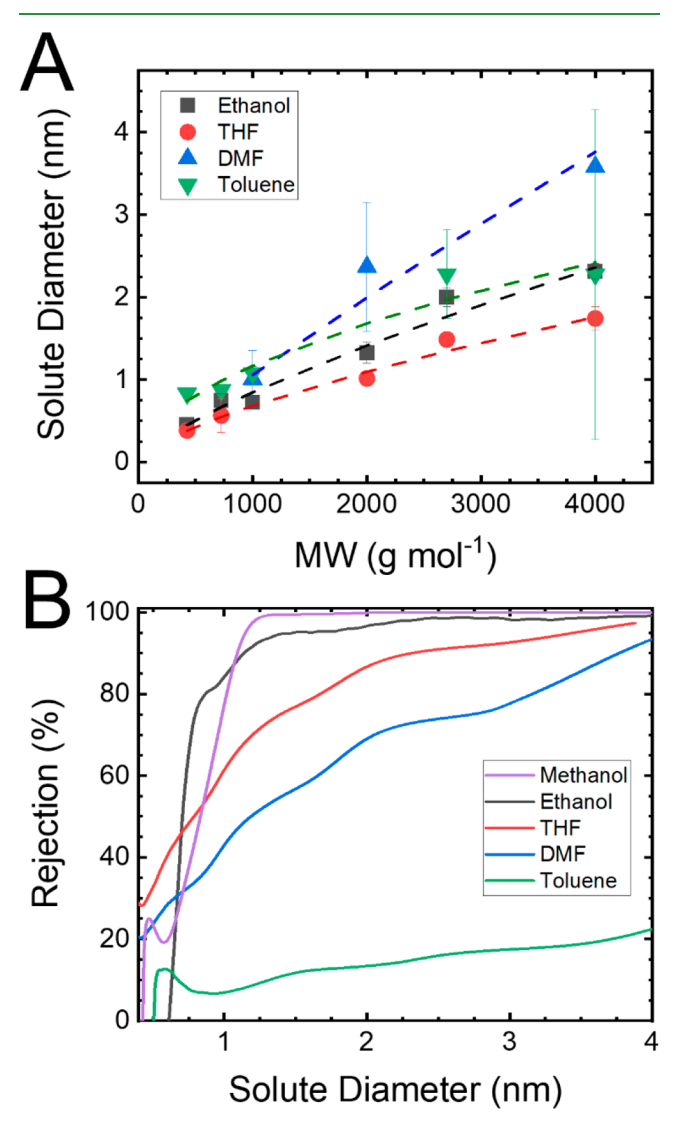


**Figure 8.** (A) DLS analysis of the PPG polymers within each solvent. Each data point is an average of n=3 measurements. The errors correspond to the standard deviation. (B) Rejection curves for diaminohexane-reacted membranes. The curves were manipulated by using a 74-point moving average to remove artifacts from the GPC results used to construct the curves. The solute diameter was determined from the DLS results. The solvated diameter of MeOH was calculated by using the DLS results for EtOH.

from 0.5 to 3.5 nm depending on the MW of the PPG molecule and the solvent identity. The similarities of the curves suggest that the PPG molecules assumed a similar size in all of the solvents tested. A power law was used to describe the relationship between the sample MW and solute diameter 57,59 when constructing the rejection curves.

The copolymer membranes were used to filter a feed solution containing 5 different MWs of PPG. GPC was then used to quantify the concentration of PPG in the feed and permeate solutions. Example traces are provided as Figures S14–S16. The signal intensity from the refractive index detector correlates with the concentration of solutes, thereby

allowing rejection to be determined using the ratio of the peak intensities. <sup>24,25</sup> For example, when the feed and permeate intensities are similar, the rejection is low. In contrast, when the permeate intensity is considerably lower than the feed intensity, the rejection of the solute is high.

The data collected through GPC were used to construct rejection curves, as shown in eq 3. The dispersity of the PPG samples resulted in a distribution of solute concentrations. In turn, the GPC analysis exhibit maxima and minima. To compensate for the waveform that appears as a result of this distribution (Figure S17), a 74-point moving average was used to smooth the curves and minimize this artifact. This 74-point moving average, which corresponded to a range of ~105 g mol<sup>-1</sup> (~0.1 nm in solvated size), was used because it gave an optically smooth curve while limiting the number of data points in the averaging process. Finally, the rejection data were combined with the results from DLS analysis so that solute rejection could be reported as a function of solute size (Figure 8B).

The plots of rejection vs solute diameter displayed in Figure 8B allow the size of permeable solvent-swollen domains within the membrane to be determined as a function of solvent identity. The MeOH and EtOH rejection curves increases sharply and reaches 90% rejection for solutes that are ~1.2 nm diameters, indicative of a well-defined nanostructure. The rejection curves collected for THF and DMF feed solutions slope more gradually and show 69% and 49% rejections, respectively, for solutes 1.2 nm in diameter. The toluene curve appears as an almost flat line near 0% rejection. These experimental results were compared to rejection curves predicted by hindered transport theory. <sup>26</sup> As shown in Figure S18, the rejection is plotted as a function of the solute diameter normalized by the pore diameter. The pore diameter, which is defined as the size of the solvent-swollen domains that contain solvated polymer chains, was an adjustable fit parameter to minimize the residual squares between the theoretical predictions and the experimental data. The resulting plot shows that EtOH rejections are best predicted, while THF, DMF, and toluene experimental rejections diverge farther from the theoretical predictions. These rejection curves suggest that as the solvent environment is changed from EtOH to toluene, the pore diameters increase (Table 2) and become less welldefined (i.e., broader in their distribution).

When the pore diameters estimated from neutral solute rejection experiments are compared with the results of the solvent permeability experiments, the permeability appears to

Table 2. Comparison of the Pore Diameter Determined through Neutral Solute Reaction and SAXS OEGMA and TFEMA Regions as a Function of Solvent for Diaminohexane-Reacted Films<sup>a</sup>

solvent	permeability factor	neutral solute (nm)	SAXS characteristic length (nm)
water	1.00	1.8 <sup>11</sup>	7.3
MeOH	0.76	1.4	N/A
EtOH	0.55	1.4	8.5
THF	0.28	2.3	9.8
DMF	0.20	3.0	7.7
toluene	0.26	9.6	8.1

<sup>&</sup>lt;sup>a</sup>The errors were not included in the comparison as they are shown in previous sections.

decrease as the pore diameter increases. This trend is unexpected, as prior work establishes that increasing pore size typically yields higher permeabilities. Therefore, SAXS analysis was conducted to probe the nanostructure of the membrane as a function of solvent. Figure S19 shows the SAXS spectra of the diaminohexane-reacted films in each solvent. The baseline scattering caused by the organic solvent was subtracted from the copolymer spectrum. The spectrum from each film exhibits one broad peak that is characteristic of a disordered, microphase-separated material. The maximum intensity of the peak is labeled with a triangular marker that indicates the representative q value for that sample. This qvalue is associated with a characteristic dimension between the scattering entities, which for this material is assumed to be the length associated with the change in density between the solvent-swollen OEGMA and TFEMA domains. All of the spectra have a broad peak around a q value of  $\sim 0.064-0.086$  $Å^{-1}$  indicative of a structure with a characteristic size of 7–9 nm. Within this range, the q value shifts depending on the solvent identity. Specifically, the q value decreases as the solvent is changed from water to EtOH to THF and then increases as the solvent is changed from THF to DMF to toluene. This trend is associated with an increase in the characteristic size of the copolymer structure and then a corresponding decrease.

Comparing these results with the tabulated  $\chi$  values for OEGMA and TFEMA, the observed changes in characteristic length may arise from the relative swelling of each domain. For the protic solvents (i.e., water and EtOH) that can hydrogen bond with the ethylene glycol repeat units, 60 solvation of the OEGMA domains is favored. For the aprotic solvents, the  $\chi$ parameter for OEGMA steadily increases, suggesting less favorable interactions between the domain and the solvents. Conversely, the  $\chi$  parameter between the solvents and TFEMA exhibits a steady decrease across the sequence of solvents mentioned above. These observations suggest that a balance exists between the swelling of the OEGMA and TFEMA domains. In solvents such as water and EtOH, primarily, the OEGMA is solvated. THF has an affinity for both of the domains, causing them to swell and leading to an increase in the structure size. For DMF and toluene, TFEMA solvation dominates swelling, leading to a reduction in the structure size. This shift in solvation could explain why limited swelling was observed in the bulk volumetric swelling experiments.

The characteristic sizes observed in the SAXS analysis can be compared with the results from neutral solute rejections to help elucidate how the OEGMA and TFEMA domains contribute to transport. The SAXS analysis suggests that the characteristic length associated with the microphase separated copolymer remained around 7.3-9.8 nm. Over the same sequence of solvents, the neutral solute rejection experiments indicate that the characteristic size of the permeable domain increased from 1.4 to 9.6 nm. For protic solvents, which interact favorably with the OEGMA domains, the characteristic size of the permeable domains compares well with limiting estimates for the size of the OEGMA domains made from the SAXS data. For instance, the water-swollen sample has an OEGMA characteristic length of 2.0 nm, similar to pore diameters calculated from neutral solute rejection in previous studies (1.8 nm).<sup>11</sup> This estimate relies on assuming a lamellar structure and that the volume fraction of OEGMA was equal to the value determined from  ${}^{1}H$  NMR analysis (~27%). ${}^{11,61}$  The characteristic size of the phase-separated structure increases

**ACS Applied Polymer Materials** 

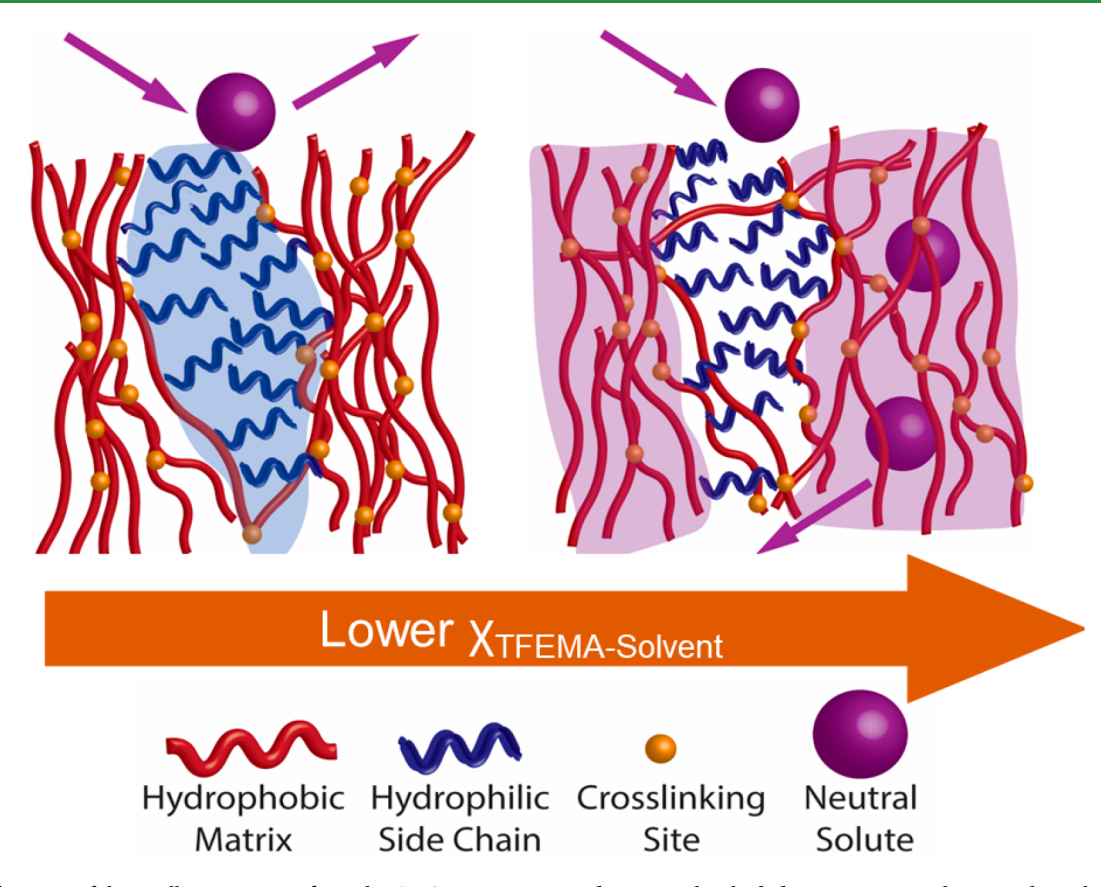


**Figure 9.** Schematic of the swelling transition from the OEGMA to TFEMA domains. The shaded areas represent the area where the copolymer is solvated. When the OEGMA domain is solvated with a protic solvent, the solvent can hydrogen bond and lubricate the domain, causing a higher permeability. As the interactions with the TFEMA become more favorable, such as with an aprotic solvent, the backbone structure experiences segmental motion, which allows for larger solutes to permeate. However, the longer chains and cross-linking throughout the structure increases the resistance for the solvent to permeate the film, causing a lower permeability compared to the OEGMA-dominated transport.

slightly as the solvent is changed from EtOH to THF, and there is a corresponding increase in the size of the permeable domain assessed using neutral solute rejection experiments. For DMF and toluene, the SAXS and neutral solute rejection size estimates diverge. With toluene, for example, the size of the permeable domain calculated from the neutral solute rejection data is slightly larger than the size of the domain attributed to the phase-separated structure from the SAXS analysis. This observation suggests that transport through TFEMA is important when toluene is used as a solvent. The value of the Flory–Huggins  $\chi$  parameter of TFEMA and toluene ( $\chi=0.12$ ) supports this claim.

The variable intensity of the broad peaks observed in the SAXS spectra also supports the assertions made regarding the solvent distribution between the OEGMA and TFEMA domains. Peak intensity correlates with the contrast among the scattering entities. The scattering length density difference between OEGMA and TFEMA is moderate, and the intensity of the peak for a dry membrane sample is small. 11 However, the solvents have scattering length densities that are distinct from those of the polymer materials. Therefore, the preferential swelling of one domain can increase the scattering contrast and lead to higher peak intensities. The SAXS spectra of the water- and toluene-swollen samples exhibit higher peak intensities, which could be a result of this swelling-induced contrast.<sup>62</sup> For solvents that do not exhibit a preferential affinity for either domain, such as THF, the peak intensity from SAXS analysis is noticeably diminished.

SAXS analysis in conjunction with neutral solute rejection experiments reveals that both copolymer domains can play an integral part in the transport of the solvent and solute. The schematic in Figure 9 tries to illustrate the transition of permeable domains within the copolymer film. When the solvent favors OEGMA, the side chains swell, while the backbone of the polymer remains relatively rigid. Additionally, the solvent molecules structure along the side chains, which then acts as a lubricative layer for the solvent to permeate through the OEGMA domain. 51,52 This solvation behavior causes the OEGMA domain to act as a pore, which allows protic solvents to permeate and only smaller neutral solutes to pass. As the solvent is changed, and the interactions between TFEMA and the solvent become more favorable, the matrix becomes solvated, and the TFEMA backbone can move more freely. The mobility of the solvated chains results in transient voids, which allow for larger neutral solutes to pass through the membrane to open. However, the backbone polymeric structure limits the transport of solvent through the membrane due to entanglement and cross-linking causing the lower permeability. This limitation becomes most apparent for toluene, where transport through the TFEMA domain dominates. The results of the neutral solute rejection experiments suggest large open voids; however, the permeability is lowest.

The claim that the solvent-swollen OEGMA domains function as pores in protic solvents is supported by a scaling analysis. For a pore-flow mechanism, the permeability is

proportional to the size of the void space (i.e., the pore diameter or spacing between polymer chains) squared. <sup>18,31,33,34,37,63-65</sup> Therefore, the permeability factors were plotted with the square of the pore diameters determined from neutral solute experiments in Figure S20. The results of experiments conducted with methanol, ethanol, and water are consistent with this scaling, which in addition to the sharp neutral solvent rejection curves suggests that these three solvents permeate through the solvated OEGMA domain via a pore-flow mechanism. The other solvents studied are not consistent with this scaling and fall on a flat line as seen in Figure S20, which suggests that these solvents do not follow a pore-flow mechanism. These observations suggest that protic solvents permeate through the copolymer via a pore-flow mechanism in the OEGMA domain, while aprotic solvents permeate through the TFEMA domain by another mechanism.

#### 4. CONCLUSION

The experiments in this study have shown that there is a correlation among the chemical properties of the copolymer, the choice of functionalization, and the transport behavior resulting from how the membrane nanostructure is affected by the polymer-solvent interactions. The repeat units used to construct the copolymer allow for different domains to be formed in the membrane, resulting in a nanostructure that permeates solvents based on the solvent-polymer affinity. Reacting the membrane with varying lengths of diamines affects the cross-linking, and therefore the resiliency, of the membrane, as seen in cycling and transport experiments. Permeability and swelling studies allowed the polymer-solvent interactions to be further investigated, showing how the OEGMA can utilize hydrogen bonding to promote the solvent transport of protic solvents. The use of SAXS and neutral solute rejection experiments allowed the nanostructure to be explored, which helped to elucidate the membrane's transition from OEGMA-dominated transport to permeation through the TFEMA domain. Understanding how the physical and chemical properties of the repeat units, the solvents, and the functionalities affect the nanostructure and performance of the OSN membranes helps to better fabricate and expand the usefulness of membranes for organic solvent-based separations.

#### ASSOCIATED CONTENT

#### **Supporting Information**

The Supporting Information is available free of charge at https://pubs.acs.org/doi/10.1021/acsapm.3c00460.

<sup>1</sup>H NMR and GPC copolymer characterization; diamine reaction schematic, FTIR and XPS analysis; permeability and swelling analysis; Flory—Huggins interaction parameter calculations; dye rejection; GPC traces from neutral solute rejections; hindered transport analysis; SAXS spectra; additional experimental details (PDF)

#### AUTHOR INFORMATION

#### **Corresponding Author**

William A. Phillip — Department of Chemical and Biomolecular Engineering, University of Notre Dame, Notre Dame, Indiana 46556, United States; orcid.org/0000-0001-8871-585X; Email: wphillip@nd.edu

#### **Authors**

- Michael P. Dugas Department of Chemical and Biomolecular Engineering, University of Notre Dame, Notre Dame, Indiana 46556, United States
- Shukun Zhong Department of Chemical and Biomolecular Engineering, University of Notre Dame, Notre Dame, Indiana 46556, United States
- Bumjun Park Department of Chemical and Biomolecular Engineering, University of Notre Dame, Notre Dame, Indiana 46556, United States; orcid.org/0000-0002-3779-1315
- Jizhou Jiang Department of Chemical and Biomolecular Engineering, University of Notre Dame, Notre Dame, Indiana 46556, United States
- Jonathan A. Ouimet Department of Chemical and Biomolecular Engineering, University of Notre Dame, Notre Dame, Indiana 46556, United States
- Jialing Xu Department of Chemical and Biomolecular Engineering, University of Notre Dame, Notre Dame, Indiana 46556, United States
- Jennifer L. Schaefer Department of Chemical and Biomolecular Engineering, University of Notre Dame, Notre Dame, Indiana 46556, United States; ○ orcid.org/0000-0003-4293-6328

Complete contact information is available at: https://pubs.acs.org/10.1021/acsapm.3c00460

#### Notes

The authors declare no competing financial interest.

#### ACKNOWLEDGMENTS

This work was made possible with support from the National Science Foundation (NSF) (Award Number: 1932206), and we appreciatively acknowledge this support. The authors acknowledge the Notre Dame Center for Environmental Science and Technology (CEST) and the Notre Dame Integrated Imaging Facility (NDIIF) for the use of instruments to perform experiments. This research also used resources of the Advanced Photon Source, a U.S. Department of Energy (DOE) Office of Science User Facility operated for the DOE Office of Science by Argonne National Laboratory under Contract DE-AC02-06CH11357. M.P.D. gratefully acknowledges support from the CEST/Bayer Predoctoral Fellowship and the Patrick and Jana Eilers Graduate Student Fellowship for Energy Related Research from Notre Dame Energy at the University of Notre Dame.

#### REFERENCES

- (1) Koros, W. J. Evolving beyond the Thermal Age of Separation Processes: Membranes Can Lead the Way. *AIChE J.* **2004**, *50* (10), 2326–2334.
- (2) Sholl, D. S.; Lively, R. P. Seven Chemical Separations to Change the World. *Nature* **2016**, 532 (7600), 435–437.
- (3) Noble, R. D.; Agrawal, R. Separations Research Needs for the 21st Century. *Ind. Eng. Chem. Res.* **2005**, 44 (9), 2887–2892.
- (4) Lively, R. P.; Sholl, D. S. From Water to Organics in Membrane Separations: Membrane Materials Provide Economical Means to Achieve Various Separation Processes And Their Capabilities for Processing Organic Fluids Look Set to Expand Significantly. *Nat. Mater.* **2017**, *16* (3), 276–279.
- (5) Xu, S.; Wang, Z. Y.; Li, S.; Tian, L.; Su, B. Fabrication of Polyimide-Based Hollow Fiber Membrane by Synergetic Covalent-Crosslinking Strategy for Organic Solvent Nanofiltration (OSN) Application. Sep. Purif. Technol. 2020, 241, 116751.

- (6) Li, C.; Li, S.; Lv, L.; Su, B.; Hu, M. Z. High Solvent-Resistant and Integrally Crosslinked Polyimide-Based Composite Membranes for Organic Solvent Nanofiltration. *J. Membr. Sci.* **2018**, *564* (June), 10–21.
- (7) Hendrix, K.; Vanherck, K.; Vankelecom, I. F. J. Optimization of Solvent Resistant Nanofiltration Membranes Prepared by the In-Situ Diamine Crosslinking Method. *J. Membr. Sci.* **2012**, 421–422, 15–24.
- (8) Xu, Y. C.; Cheng, X. Q.; Long, J.; Shao, L. A Novel Monoamine Modification Strategy toward High-Performance Organic Solvent Nanofiltration (OSN) Membrane for Sustainable Molecular Separations. *J. Membr. Sci.* **2016**, *497*, 77–89.
- (9) Bates, F. S.; Hillmyer, M. A.; Lodge, T. P.; Bates, C. M.; Delaney, K. T.; Fredrickson, G. H. Multiblock Polymers: Panacea or Pandora's Box? *Science* **2012**, 336 (6080), 434–440.
- (10) Qu, S.; Dilenschneider, T.; Phillip, W. A. Preparation of Chemically-Tailored Copolymer Membranes with Tunable Ion Transport Properties. *ACS Appl. Mater. Interfaces* **2015**, 7 (35), 19746–19754.
- (11) Dugas, M. P.; Van Every, G.; Park, B.; Hoffman, J. R.; Larue, R. J.; Bush, A. M.; Zhang, Y.; Schaefer, J. L.; Latulippe, D. R.; Phillip, W. A. Resilient Hollow Fiber Nanofiltration Membranes Fabricated from Crosslinkable Phase-Separated Copolymers. *Molecular Systems Design and Engineering* **2020**, *5* (5), 943–953.
- (12) Lounder, S. J.; Asatekin, A. Fouling- and Chlorine-Resistant Nanofiltration Membranes Fabricated from Charged Zwitterionic Amphiphilic Copolymers. *ACS Appl. Polym. Mater.* **2022**, *4*, 7998.
- (13) Sadeghi, I.; Asatekin, A. Spontaneous Self-Assembly and Micellization of Random Copolymers in Organic Solvents. *Macromol. Chem. Phys.* **2017**, 218 (20), 1–9.
- (14) Bengani, P.; Kou, Y.; Asatekin, A. Zwitterionic Copolymer Self-Assembly for Fouling Resistant, High Flux Membranes with Size-Based Small Molecule Selectivity. *J. Membr. Sci.* **2015**, 493, 755–765.
- (15) Qu, S.; Shi, Y.; Benavides, S.; Hunter, A.; Gao, H.; Phillip, W. A. Copolymer Nanofilters with Charge-Patterned Domains for Enhanced Electrolyte Transport. *Chem. Mater.* **2017**, 29 (2), 762–772.
- (16) Petersen, R. J. Composite Reverse Osmosis and Nanofiltration Membranes. J. Membr. Sci. 1993, 83 (1), 81–150.
- (17) Hoffman, J. R.; Phillip, W. A. Dual-Functional Nanofiltration Membranes Exhibit Multifaceted Ion Rejection and Antifouling Performance. ACS Appl. Mater. Interfaces 2020, 12 (17), 19944—19954.
- (18) Marchetti, P.; Jimenez Solomon, M. F.; Szekely, G.; Livingston, A. G. Molecular Separation with Organic Solvent Nanofiltration: A Critical Review. *Chem. Rev.* **2014**, *114* (21), 10735–10806.
- (19) Rathee, V. S.; Qu, S.; Phillip, W. A.; Whitmer, J. K. A Coarse-Grained Thermodynamic Model for the Predictive Engineering of Valence-Selective Membranes. *Molecular Systems Design & Engineering* **2016**, *1* (3), 301–312.
- (20) Ball, V. Polydopamine Nanomaterials: Recent Advances in Synthesis Methods and Applications. Frontiers in Bioengineering and Biotechnology 2018, 6 (AUG), 1–12.
- (21) El Yakhlifi, S.; Ihiawakrim, D.; Ersen, O.; Ball, V. Enzymatically Active Polydopamine @ Alkaline Phosphatase Nanoparticles Produced by NaIO4 Oxidation of Dopamine. *Biomimetics* **2018**, 3 (4), 1–23.
- (22) Barbey, R.; Laporte, V.; Alnabulsi, S.; Klok, H. A. Postpolymerization Modification of Poly(Glycidyl Methacrylate) Brushes: An XPS Depth-Profiling Study. *Macromolecules* **2013**, 46 (15), 6151–6158.
- (23) Miranda, A.; Martínez, L.; De Beule, P. A.A. Facile Synthesis of an Aminopropylsilane Layer on Si/SiO<sub>2</sub> Substrates Using Ethanol as APTES Solvent. *MethodsX* **2020**, *7*, 100931.
- (24) Hong, M.; Liu, W.; Liu, Y.; Dai, X.; Kang, Y.; Li, R.; Bao, F.; Qiu, X.; Pan, Y.; Ji, X. Improved Characterization on Molecular Weight of Polyamic Acids Using Gel Permeation Chromatography Coupled with Differential Refractive Index and Multi-Angle Laser Light Scattering Detectors. *Polymer* **2022**, *260*, 125370.

- (25) Xu, M.; Li, D.-S.; Li, B.; Wang, C.; Zhu, Y.-P.; Lv, W.-P.; Xie, B.-J. Comparative Study on Molecular Weight of Konjac Glucomannan by Gel Permeation Chromatography-Laser Light Scattering-Refractive Index and Laser Light-Scattering Methods. *Journal of Spectroscopy* **2013**, 2013, 1–4.
- (26) Zeman, L.; Wales, M. Steric Rejection of Polymeric Solutes by Membranes with Uniform Pore Size Distribution. *Sep. Sci. Technol.* **1981**, *16* (3), 275–290.
- (27) Benavides, S.; Qu, S.; Gao, F.; Phillip, W. A. Polymeric Ion Pumps: Using an Oscillating Stimulus to Drive Solute Transport in Reactive Membranes. *Langmuir* **2018**, *34* (15), 4503–4514.
- (28) Zhang, Y.; Sargent, J. L.; Boudouris, B. W.; Phillip, W. A. Nanoporous Membranes Generated from Self-Assembled Block Polymer Precursors: Quo Vadis? *J. Appl. Polym. Sci.* **2015**, *132* (21), 1–17.
- (29) Ravi, N.; Mitra, A.; Hamilton, P.; Horkay, F. Characterization of the Network Properties of Poly(Ethylene Glycol)-Acrylate Hydrogels Prepared by Variations in the Ethanol-Water Solvent Composition during Crosslinking Copolymerization. *J. Polym. Sci., Part B: Polym. Phys.* **2002**, *40* (23), 2677–2684.
- (30) Wijmans, J. G. The Role of Permeant Molar Volume in the Solution-Diffusion Model Transport Equations. J. Membr. Sci. 2004, 237 (1–2), 39–50.
- (31) Li, Y.; Zhu, J.; Li, S.; Guo, Z.; Van Der Bruggen, B. Flexible Aliphatic-Aromatic Polyamide Thin Film Composite Membrane for Highly Efficient Organic Solvent Nanofiltration. *ACS Appl. Mater. Interfaces* **2020**, *12* (28), 31962–31974.
- (32) MacHado, D. R.; Hasson, D.; Semiat, R. Effect of Solvent Properties on Permeate Flow through Nanofiltration Membranes. Part I: Investigation of Parameters Affecting Solvent Flux. *J. Membr. Sci.* 1999, 163 (1), 93–102.
- (33) Fujiyabu, T.; Li, X.; Shibayama, M.; Chung, U. Il; Sakai, T. Permeation of Water through Hydrogels with Controlled Network Structure. *Macromolecules* **2017**, *50* (23), 9411–9416.
- (34) Tokita, M.; Tanaka, T. Friction Coefficient of Polymer Networks of Gels. J. Chem. Phys. 1991, 95 (6), 4613-4619.
- (35) Buekenhoudt, A.; Bisignano, F.; De Luca, G.; Vandezande, P.; Wouters, M.; Verhulst, K. Unravelling the Solvent Flux Behaviour of Ceramic Nanofiltration and Ultrafiltration Membranes. *J. Membr. Sci.* **2013**, 439, 36–47.
- (36) Silva, P.; Han, S.; Livingston, A. G. Solvent Transport in Organic Solvent Nanofiltration Membranes. *J. Membr. Sci.* **2005**, 262 (1–2), 49–59.
- (37) Baker, R. W. Membrane Technology and Applications, 2nd ed.; John Wiley & Sons: 2004; pp 18-85.
- (38) Paul, D. R. Reformulation of the Solution-Diffusion Theory of Reverse Osmosis. *J. Membr. Sci.* **2004**, *241* (2), 371–386.
- (39) Vrentas, J. S.; Duda, J. L. Solvent and Temperature Effects on Diffusion in Polymer-Solvent Systems. *J. Appl. Polym. Sci.* 1977, 21 (6), 1715–1728.
- (40) Zafarani-Moattar, M. T.; Sarmad, S. Measurement and Correlation of Phase Equilibria for Poly(Ethylene Glycol) Methacrylate + Alcohol Systems at 298.15 K. *Journal of Chemical & Engineering Data* 2005, 50 (1), 283–287.
- (41) Özdemir, C.; Güner, A. Solubility Profiles of Poly(Ethylene Glycol)/Solvent Systems, I: Qualitative Comparison of Solubility Parameter Approaches. *Eur. Polym. J.* **2007**, *43* (7), 3068–3093.
- (42) Papadopoulou, S. K.; Panayiotou, C. Assessment of the Thermodynamic Properties of Poly(2,2,2-Trifluoroethyl Methacrylate) by Inverse Gas Chromatography. *Journal of Chromatography A* **2014**, 1324, 207–214.
- (43) Phillip, W. A.; O'neill, B.; Rodwogin, M.; Hillmyer, M. A.; Cussler, E. L. Self-Assembled Block Copolymer Thin Films as Water Filtration Membranes. *ACS Appl. Mater. Interfaces* **2010**, 2 (3), 847–852
- (44) Hansen, C. M. Hansen Solubility Parameters: A User's Handbook, 2nd ed.; CRC Press: 2007.
- (45) Soroko, I.; Lopes, M. P.; Livingston, A. The Effect of Membrane Formation Parameters on Performance of Polyimide

- Membranes for Organic Solvent Nanofiltration (OSN): Part A. Effect of Polymer/Solvent/Non-Solvent System Choice. *J. Membr. Sci.* **2011**, 381 (1–2), 152–162.
- (46) Evans, K. M.; Hardy, J. K. Predicting Solubility and Permeation Properties of Organic Solvents in Viton Glove Material Using Hansen's Solubility Parameters. *J. Appl. Polym. Sci.* **2004**, 93 (6), 2688–2698.
- (47) Su, X.; Shi, B.; Wang, L. Investigation on Three-Dimensional Solubility Parameters for Explanation and Prediction of Swelling Degree of Polydimethylsiloxane Pervaporation Membranes. *Journal of Macromolecular Science, Part B* **2015**, 54 (10), 1248–1258.
- (48) Kawaguchi, S.; Imai, G.; Suzuki, J.; Miyahara, A.; Kitano, T.; Ito, K. Aqueous Solution Properties of Oligo- and Poly(Ethylene Oxide) by Static Light Scattering and Intrinsic Viscosity. *Polymer* 1997, 38 (12), 2885–2891.
- (49) Kjellander, R.; Florin, E. Water Structure and Changes in Thermal Stability of the System Poly(Ethylene Oxide)-Water. J. Chem. Soc., Faraday Transactions 1: Physical Chemistry in Condensed Phases 1981, 77 (9), 2053–2077.
- (50) Alexandridis, P.; Alan Hatton, T. Poly(Ethylene Oxide)Poly-(Propylene Oxide)Poly(Ethylene Oxide) Block Copolymer Surfactants in Aqueous Solutions and at Interfaces: Thermodynamics, Structure, Dynamics, and Modeling. *Colloids Surf., A* **1995**, *96* (1–2), 1–46.
- (51) Brown, W. Diffusion of Poly(Ethylene Oxide) in Semidilute Aqueous Solution: Dynamic Light Scattering and Gradient Diffusion. *Polymer* 1985, 26 (11), 1647–1650.
- (52) Zheng, X.; Anisimov, M. A.; Sengers, J. V.; He, M. Mesoscopic Diffusion of Poly(Ethylene Oxide) in Pure and Mixed Solvents. *J. Phys. Chem. B* **2018**, *122* (13), 3454–3464.
- (53) Peyravi, M.; Rahimpour, A.; Jahanshahi, M. Thin Film Composite Membranes with Modified Polysulfone Supports for Organic Solvent Nanofiltration. *J. Membr. Sci.* **2012**, 423–424, 225–237.
- (54) Geens, J.; Peeters, K.; Van Der Bruggen, B.; Vandecasteele, C. Polymeric Nanofiltration of Binary Water-Alcohol Mixtures: Influence of Feed Composition and Membrane Properties on Permeability and Rejection. *J. Membr. Sci.* **2005**, *255* (1–2), *255*–264.
- (55) Li, X.; Vandezande, P.; Vankelecom, I. F. J. Polypyrrole Modified Solvent Resistant Nanofiltration Membranes. *J. Membr. Sci.* **2008**, 320 (1–2), 143–150.
- (56) Davey, C. J.; Low, Z.-X.; Wirawan, R. H.; Patterson, D. A. Molecular Weight Cut-off Determination of Organic Solvent Nanofiltration Membranes Using Poly(Propylene Glycol). *J. Membr. Sci.* **2017**, *526*, 221–228.
- (57) Sandell, L. S.; Goring, D. A. I. Solvent-Induced Conformational Expansion of Oligomeric Propylene Glycols. *Macromolecules* **1970**, 3 (1), 54–57.
- (58) Sandell, L. S.; Goring, D. A. I. A Comparison of the Intrinsic Viscosities of Oligomeric Propylene Glycols with the Behavior Predicted for Models in Aqueous Solution at 25°. *Macromolecules* 1970, 3 (1), 50–54.
- (59) Polik, W. F.; Burchard, W. Static Light Scattering from Aqueous Poly(Ethylene Oxide) Solutions in the Temperature Range 20–90 °C. *Macromolecules* **1983**, *16* (6), 978–982.
- (60) Lodge, T. P.; Hiemenz, P. C. Polymer Chemistry, 2nd ed.; CRC Press: Boca Raton, FL, 2020.
- (61) Bush, A. M.; Ford, H. O.; Gao, F.; Summe, M. J.; Rouvimov, S.; Schaefer, J. L.; Phillip, W. A.; Guo, R. Tunable Mesoporous Films from Copolymers with Degradable Side Chains as Membrane Precursors. J. Membr. Sci. 2018, 567, 104–114.
- (62) Chu, B.; Hsiao, B. S. Small-Angle X-Ray Scattering of Polymers. *Chem. Rev.* **2001**, *101* (6), 1727–1761.
- (63) Annaka, M.; Tanaka, T. Condition for Multiple Phases of Polymer Gels. *Phase Transitions* **1994**, 47 (3-4), 143-159.
- (64) Darvishmanesh, S.; Tasselli, F.; Jansen, J. C.; Tocci, E.; Bazzarelli, F.; Bernardo, P.; Luis, P.; Degrève, J.; Drioli, E.; Van der Bruggen, B. Preparation of Solvent Stable Polyphenylsulfone Hollow

Fiber Nanofiltration Membranes. J. Membr. Sci. 2011, 384 (1-2), 89-96.

(65) Darvishmanesh, S.; Degrève, J.; Van Der Bruggen, B. Mechanisms of Solute Rejection in Solvent Resistant Nanofiltration: The Effect of Solvent on Solute Rejection. *Phys. Chem. Chem. Phys.* **2010**, *12* (40), 13333–13342.

### **□** Recommended by ACS

## Stiffening Polymer Brush Membranes for Enhanced Organic Solvent Nanofiltration Selectivity

Pranav Ramesh, Georges Belfort, et al.

JUNE 21, 2023

ACS APPLIED MATERIALS & INTERFACES

READ 🗹

#### Surface Modification of Nanofiltration Membranes by Interpenetrating Polymer Networks and Their Evaluation in Water Desalination

C. Vargas-Figueroa, R. Borquez, et al.

JUNE 02, 2023

ACS APPLIED POLYMER MATERIALS

READ 🗹

## Poly(methyl methacrylate)-block-polysulfone-poly(methyl methacrylate) Triblock Copolymer-Modified Support Layers for Forward Osmosis Membranes

Alireza Farazin, Hossein Mahdavi, et al.

OCTOBER 19, 2023

ACS APPLIED POLYMER MATERIALS

READ **C** 

## **Zwitterionic Copolymers for Anti-Scaling Applications in Simulated Spaceflight Wastewater Scenarios**

Elisabeth R. Thomas, Mary Laura Lind, et al.

MAY 15, 2023

ACS OMEGA

READ 🗹

Get More Suggestions >